

On the role of dynamical barriers in barrierless-reactions at low energies: $S(^1D) + H_2$ Manuel Lara*,¹ P. G. Jambrina,² A. J. C. Varandas^{†,3} J.-M. Launay^{‡,4} and F. J. Aoiz^{§5}¹ *Departamento de Química Física, Facultad de Química, Universidad Complutense, 28040 Madrid, Spain
Institut de Physique de Rennes, UMR CNRS 6251,
Université de Rennes I, F-35042 Rennes, France*² *Departamento de Química Física, Facultad de Química, Universidad Complutense, 28040 Madrid, Spain
Grupo de Dinámica Molecular. Departamento de Química Física,
Universidad de Salamanca, 37008 Salamanca, Spain*³ *Departamento de Química, Universidade de Coimbra, 3004-535 Coimbra, Portugal*⁴ *Institut de Physique de Rennes, UMR CNRS 6251,
Université de Rennes I, F-35042 Rennes, France*⁵ *Departamento de Química Física, Facultad de Química, Universidad Complutense, 28040 Madrid, Spain
(Dated: July 25, 2018)*

Reaction probabilities as a function of total angular momentum (opacity functions) and the resulting reaction cross-sections for the collision of open shell $S(^1D)$ atoms with *para*-hydrogen have been calculated in the kinetic energy range 0.09–10 meV (1–120 K). The quantum mechanical (QM) hyperspherical reactive scattering method and quasi-classical trajectory (QCT) and statistical quasiclassical trajectory (SQCT) approaches were used. Two different *ab initio* potential energy surfaces (PESs) have been considered. The widely used RKHS PES by Ho *et al.* (*J. Chem. Phys.* **116**, 4124, 2002) and the recently published DMBE/CBS PES by Song and Varandas (*J. Chem. Phys.* **130**, 134317, 2009). The calculations at low collision energies reveal very different dynamical behaviors on the two PESs. The reactivity on the RKHS PES is found to be considerably larger than that on the DMBE/CBS PES as a result of larger reaction probabilities at low total (here also orbital) angular momentum values and to opacity functions which extend to significantly larger total angular momentum values. The observed differences have their origin in two major distinct topography features. Although both PESs are essentially barrierless for equilibrium H–H distances, when the H–H bond is compressed the DMBE/CBS PES gives rise to a dynamical barrier which limits the reactivity of the system. This barrier is completely absent in the RKHS PES. In addition, the latter PES exhibits a van der Waals well in the entrance channel which reduces the height of the centrifugal barrier and is able to support resonances. As a result a significant larger cross section is found on this PES, with marked oscillations attributable to shape resonances and/or to the opening of partial wave contributions. The comparison of the results on both PESs is illustrative of the wealth of the dynamics at low collision energy. It is also illuminating about the difficulties encountered in modelling an all-purpose global potential energy surface.

PACS numbers:

I. INTRODUCTION

The advent of experimental techniques that allow the cooling of translational degrees of freedom has paved the way for obtaining data on reactive processes at very low temperatures and kinetic energies. In particular, the CRESU (Reaction Kinetics in Uniform Supersonic Flow) technique [1, 2], implemented in Rennes, and crossed molecular beam techniques with variable beam intersection-angle, as that in Bordeaux [2, 3], can be used to explore reactions of atomic radicals such as $F(^2P_J)$, $C(^1D_2)$, $O(^1D_2)$, $S(^1D_2)$ with H_2 at translational colli-

sion energies, E_{coll} , down to fractions of meV or, equivalently, few K ($1\text{K} \approx 8.6 \times 10^{-5}\text{eV}$). This information can be of direct application to the chemistry of planetary atmospheres and dense interstellar clouds [4]. Rate constants and excitation functions for the title reaction [2, 3] at temperatures and kinetic energies as low as $\sim 5\text{K}$ have been already determined.

The new context raises questions about the capability of our theoretical methodology to handle cold ($< 1\text{K}$) and ultracold ($< 10^{-3}\text{K}$) processes which are sensitive to interactions at distances on the order of hundreds or even thousands of atomic units. As a simple rule of thumb in cold collisions, the propagation would have to be pursued to distances for which the potential energy is of the same order of the considered kinetic energy. Thereby stopping a calculation at distances on the order of $10 a_0$ – $20 a_0$ would invalidate any result for kinetic energies on the order of 10 K and, consequently, a major issue is the feasibility of a global potential energy surface (PES) to describe the whole configuration space in a balanced way. Collisions in the range ~ 10 – 100K , as those considered here, may well lie in the limits of what can be achieved

*Corresponding author. E-mail: manuel.lara@uam.es
Present address: Departamento de Química Física Aplicada, Facultad de Ciencias. Universidad Autónoma de Madrid. 28049 Madrid, Spain

[†]E-mail: varandas@qtvs1.qui.uc.pt

[‡]E-mail: jean-michel.launay@univ-rennes1.fr

[§]Corresponding author. E-mail: aoiz@quim.ucm.es

nowadays using conventional theoretical tools for atom-diatom system.

Traditionally, the long-range regions of the PESs have been largely neglected and deemed almost irrelevant for the dynamics of the reaction and in the overall reactivity. This is so, despite the fact that a method (dubbed as DMBE [5] from double many-body expansion) had been proposed more than two decades ago to formally introduce long-range forces into global potential energy surfaces for dynamics studies, both of the single- and multi-sheeted [6] types. Due to computational limitations at the time, DMBE theory assumed originally a semi-empirical foundation although it soon led to a general strategy for fitting *ab initio* potential energy surfaces encompassing both short- and long-range forces. Indeed, at sufficiently low kinetic energies, long-range interactions start playing an essential role inasmuch as they determine the amount of incoming flux which reaches the short-range region where rearrangement may occur [7, 8]. While in the thermal regime short-range chemical forces prevail rendering the long-range forces less relevant, in the cold scenario long-range interactions become of crucial importance [9]. Interestingly, dynamical studies at intermediate energies in the range $\approx 1 - 10$ K may display the combined contributions of short-range and long-range interactions [10]. In this context, collisions in this range of energies turn out to be an excellent mean to assess the quality of the PES sampling both long-range and short-range regions.

The practical study of reactions at low collision energies is obviously restricted to barrierless reactions (or with barriers low enough to allow resonance enhanced tunneling). Among them, the slightly exoergic $S(^1D) + H_2(X^1\Sigma_g^+) \rightarrow SH(X^2\Pi) + H(^2S)$ ($\Delta D_e = 0.18$ meV, $\Delta H_0^0 = -0.29$ eV) insertion reaction constitutes an excellent example [11]. On its ground potential energy surface, the $1^1A'$ electronic state, the main reaction path features a deep well (≈ 3.90 eV from the minimum of the reactant's valley). In total there are five PESs ($1^1A'$, $2^1A'$, $3^1A'$, $1^1A''$ and $2^1A''$) that correlate with the $S(^1D) + H_2$ asymptote. Of these only two, the $1^1A'$ PES and the $1^1A''$ PES, also correlate adiabatically with the products, whereas the remaining PESs are repulsive along their respective minimum energy paths connecting with excited states of the products. This fact does not preclude that other PESs could be relevant at intermediate regions, particularly via conical intersections that may call for the appearance of further non-adiabatic effects, especially at sufficiently high collision energies. The ground electronic state $1^1A'$ has no barrier for perpendicular insertion whereas the first excited $1^1A''$ PES has a considerably high collinear barrier (≈ 0.43 eV) which increases for larger angles. Thereby, at the moderate collision energies of the available experiments and moreover at low collision energies, the reaction is likely to be restricted to the ground state PES.

The title reaction and its isotopic variants at thermal energies have been the subject of detailed analysis in the

past [11–28]. The experimental measurements by Liu and coworkers [24–26] motivated a number of theoretical studies. In particular, Zyubin *et al* [12] carried out extensive MRCI *ab initio* calculations with multiconfiguration self-consistent field (MCSCF) reference wave functions for all the PESs that correlate with the reagents. Subsequently, an improved version of the $1^1A'$ PES based on the same *ab initio* points was produced by Ho *et al.* using the reproducing kernel Hilbert space (RKHS) interpolation method. The resulting PES, henceforth called RKHS PES, has no barrier for insertion but exhibits a late collinear barrier whose height is ≈ 0.36 eV. As will be seen, this barrier plays a non-negligible role in the dynamics at low E_{coll} . This PES has been extensively used in quasi-classical trajectory (QCT) [13–16], time independent quantum mechanical (TI-QM) [15, 17], wave packet [21, 27, 28], rigorous statistical quantum mechanical (SQM) [18, 20, 29] and statistical quasi-classical trajectory (SQCT) [19] dynamical calculations.

In previous studies [2, 3, 10], accurate, fully converged QM dynamical calculations were performed to explore the reactive behavior of the title reaction at low kinetic energies and to compare their results with the recent measurements by Sims and coworkers and Costes and coworkers [2, 3]. These QM calculations were carried out on the RKHS ground $1^1A'$ adiabatic PES. However, since the accent was put on the accurate reproduction of the experimental data, it was found that the short-range description of the RKHS PES required to be complemented with an *ad hoc* modification of the long-range interactions. Although the RKHS had been widely used in the past and its short-range region was tested by comparison with experiments at higher energies [15, 16], its long-range potential was not accurate enough to describe the experimental results at kinetic energies $\lesssim 10$ K, even though its effect was found negligible at higher energies. It should be recalled that the long-range behavior in the system is characterized by the presence of a significant quadrupole-quadrupole contribution that varies as R^{-5} (R being the atom-diatom distance) which is due to the open shell nature of the excited electronic state of the S atom. This potential term may lead to important reorientation effects at low collision energies.

Recently, a new *ab initio* PES for the system, named DMBE/CBS was calculated by Song and Varandas [30] by fitting accurate multireference configuration interaction energies with large basis sets (Dunning's aug-cc-pVTZ and aug-cc-pVQZ) and extrapolation to the complete basis set (CBS) limit [31]. Special care was paid in the fitting procedure to the long range behavior, although the quadrupole-quadrupole electrostatic interaction was not explicitly considered. Given the high level of *ab initio* calculations used in its construction, one can expect a higher degree of accuracy as compared with previous PESs for the ground $1^1A'$ state of the SH_2 system. The few dynamical studies available on this PES at the time [30] pointed at different dynamical effects to those calculated on the RKHS PES [14] and even with those

reported for a similar PES by the same authors [30, 32] to be addressed further below. In particular, the values of their QCT thermal rate constants at 300 K for different isotopes and intramolecular and intermolecular kinetic isotope effects were presented in ref. [30], indicating some discrepancies in the results from the previous PESs. Although, shortly after its publication, it was recognized by the authors that the tabulated experimental branching ratios (seventh column of Table 4 in Ref. [30] should read as the inverse values of the ones actually given), the above finding prompts the question about their quality and topographical differences. As commented on above, the analysis of low collision energy results is probably the most stringent test to assess the overall performance of a PES. Under such conditions the parallel study of the dynamics of a given reaction on two different PESs may serve to disentangle more or less subtle effects due to specific features of the potential. In the present study, only the original RKHS PES and DMBE/CBS PES, as they were released without modifications, will be employed. In any case, the modification of the long-range part of the RKHS PES used in ref. [2, 10] only affects the excitation functions at energies below 1 meV as it was previously shown [10].

Shortly after the publication of the DMBE/CBS PES, another PES, based essentially on the same set of *ab initio* data, was released by Varandas and coworkers: the DMBE/SEC PES [32], so called for the use of the scaled external correlation aimed to extrapolate to the complete basis set and full configuration-interaction limits [33]. A comparative study of the dynamics on both the DMBE/CBS PES and DMBE/SEC PES has been recently carried out [34] using accurate time-dependent wave packet (TD-WP) calculations. That work was performed independently and in parallel to the present one that uses different theoretical methodologies, SQCT, QCT and rigorous TI-QM, the latter more accurate than TD-WP for low collision energies. The present work is focussed on detailed comparison of the DMBE/CBS and RKHS PESs exclusively at low collision energies and to disentangle the various dynamical effects.

At lower energies in the reactant valley lie the adiabatic triplet PES that correlates with the $S(^3P)+H_2$ and crosses the $^1A'$ PES in the H_2S well, leading to the same asymptote in the product's valley. Theoretical calculations[23, 27] conclude that although the contribution to the product's formation via inter system crossing is small, the electronic non-reactive quenching process, $S(^1D) + H_2 \rightarrow S(^3P_{0,1,2}) + H_2$, may play a significant role in the absolute removal of $S(^1D)$, at least at energies as low as 250K (21.5 meV). The real contribution of the quenching to the collision process at low energies has not been cleared up by the recent experiments on the system and the resulting theoretical analysis [2, 3]. The branching ratio reaction to quenching in the considered range remains unknown. Hereinafter, we will consider purely adiabatic collisions on the ground state PES since the purpose of the present work is to isolate the effects of the

features of the ground state potential on the low energy collision dynamics. The excellent agreement between recent experimental data and adiabatic calculations in the low energy range [2, 3] indicates that the possible non-adiabatic effects mentioned above should be largely irrelevant for the measured dynamical observables (cross sections and rate coefficients) at sufficiently low collision energies.

The paper is structured as follows. In the next section, we will briefly describe the three dynamical methodologies used. The results of the calculations will be shown in Section III and will be discussed in Section IV. Finally, a summary of the work and some conclusions will be given in Section V.

II. DYNAMICAL METHODOLOGY

A. Quasi-Classical trajectory method

QCT calculations have been carried out for the $S(^1D)+H_2(v=0,j=0)$ reaction by running 10^6 trajectories in the 0.5 meV–10 meV collision energy range on each of the PES considered in this work. The integration step was chosen to be 4×10^{-17} s on the RKHS PES and 6×10^{-17} s on the DMBE/CBS PES. This guarantees a total energy conservation better than 1 part in 10^4 . Due to the small collision energies and the long range interaction in the potential, the initial and final atom-diatom distance was chosen to be 30 Å. The detailed QCT procedure has been discussed elsewhere [35, 36] and will not be repeated here.

The same methodology was employed to calculate the excitation functions for the $S + H_2(v=1,j=0)$ reaction by running 10^6 trajectories in the collision energy range between 5 meV and 500 meV. The initial atom-diatom distance was set to 10 Å. To improve the accuracy at low values of E_{coll} , an extra batch of 10^6 trajectories was run in the energy range 0.5 meV–80 meV on the RKHS PES. Additional batches of 10^5 trajectories were also run at discrete collision energies (5 meV, 6.29 meV, 10 meV and 30 meV for the reaction with $H_2(v=0,j=0)$ and 32 meV and 82 meV for the reaction with $H_2(v=1,j=0)$) using the standard QCT methodology [35] to determine the opacity functions.

The effect of the different types of binning for the assignment of final states on the cross section and opacity was also studied. Since no resolution in final states is carried out in this work, the results obtained were insensitive to the particular binning method that could be used, as also found elsewhere [32] using a related approach

B. Statistical Quasi-Classical trajectory method

The SQCT method has been described in previous publications [19, 37, 38]. It is equivalent in all aspects to its QM version, SQM [18], with the sole difference that

trajectories instead of wave functions are propagated. In the SQCT method, the trajectories are integrated until they reach the well, characterized for a negative limiting value of the potential (measured from the bottom of the reactant’s valley). Calculations for the title reaction had been already performed using the SQCT and SQM approaches [19] yielding almost identical results. In this case, the limiting value was chosen to be -0.6 eV for the reagents channel and -0.8 eV for the products.

Calculations were performed at several values of E_{coll} over the 1 meV–10 meV and 30–280 meV ranges for the $S(^1D)+\text{H}_2(v=0, j=0)$ and $S(^1D)+\text{H}_2(v=1, j=0)$ reactions, respectively. Batches of 10^5 trajectories were run for each energy and chemical rearrangement on each of the PESs. The integration step size was chosen to be 7×10^{-17} s (for both PES) enough to ensure a conservation in the total energy better than 1 part in 10^5 .

C. The Quantum mechanical hyperspherical approach

The hyperspherical quantum reactive scattering method developed by Launay *et al.* [39] was described in previous works in the context of thermal reactive scattering [40]. Recent modifications of the method performed in order to allow the accurate inclusion of small anisotropic long-range interactions in the PES were described in depth in ref. [10]. In what follows, we will simply recall the basic concepts referring to previous works for more details.

In the hyperspherical quantum reactive scattering method, developed by Launay [39], the configuration space is divided into inner and outer regions. The positions of the nuclei in the inner region are described in terms of hyperspherical democratic coordinates. The logarithmic derivative of the wavefunction is propagated outwards on a single adiabatic PES. At a large enough value of the hyper-radius the former is matched to a set of suitable functions, called asymptotic functions, to yield the scattering S-matrix. The asymptotic functions provide the collision boundary conditions. In fact, when working at thermal energies, they are the familiar regular and irregular radial Bessel functions which account for the presence of the centrifugal potential at large intermolecular separations. They were recently generalized in order to include also the effect of anisotropic long-range interactions which act on the reagents while they approach each other. This enables the study of cold and

ultracold collisions, very sensitive to the long-range part of the PES, without the need of extending the inner calculation, in hyperspherical coordinates, to very large values of the hyper-radius [10].

In the current study, we choose an adiabatic treatment of the dynamics, assuming that the collision occurs only on the ground adiabatic PES which will be labeled by $V^0(R, r, \theta)$. Using the set of Jacobi coordinates (R, r, θ) corresponding to the S+ H_2 arrangement, the nuclear Hamiltonian can be expressed as

$$\hat{H} = -\frac{\hbar^2}{2\mu} \frac{1}{R} \frac{\partial^2}{\partial R^2} R + \frac{1}{2\mu R^2} \mathbf{l}^2 - \frac{\hbar^2}{2m} \frac{1}{r} \frac{\partial^2}{\partial r^2} r + \frac{1}{2mr^2} \mathbf{j}^2. \quad (1)$$

Let us label with \mathbf{l} the orbital angular momentum of the atom with respect to the center of mass of the diatom, and with \mathbf{j} the rotational angular momentum of the latter. The total angular momentum of the nuclei (conserved in an adiabatic approach) is given by $\mathbf{J} = \mathbf{j} + \mathbf{l}$. A convenient basis in order to expand the nuclear wavefunction in the long-range region is that characterized by quantum numbers (J, M, v, j, l) , with (v, j) the rovibrational quantum numbers of the diatom, l the relative orbital angular momentum and (J, M) the total angular momentum and its projection on the Space-Fixed (SF) Z axis (represented as φ_{vjl}^{JM}). Such a SF basis set is used in the hyperspherical approach to expand the asymptotic wavefunctions, which are matched with the short-range information obtained in hyperspherical coordinates.

If the system approaches collision with quantum numbers (J, M, v_0, j_0, l_0) , we will assume that (in addition to J and M) the rovibrational quantum numbers, (v_0, j_0) , remain well conserved in the long-range region. This is justified given the large energy gap between different rovibrational states relative to the small considered collision energies. Within this approximation the nuclear wavefunction, $\Psi_{v_0 j_0 l_0}^{JM}$, can be expanded in the long-range region as

$$\Psi_{v_0 j_0 l_0}^{JM} = \sum_l \frac{F_l^{l_0}(R)}{R} \varphi_{v_0 j_0 l}^{JM}, \quad (2)$$

where all the “conserved” quantum numbers have been suppressed in the notation of the radial coefficients, $F_l^{l_0}(R)$. Introducing the expansion (2) into the time-independent Schrödinger equation associated with a total energy E , $H\Psi = E\Psi$, and using the Hamiltonian in Eq. 1, it is straightforward to obtain the following system of coupled radial equations

$$\left[-\frac{\hbar^2}{2\mu} \frac{\partial^2}{\partial R^2} + \frac{l(l+1)\hbar^2}{2\mu R^2} - E_{\text{coll}} \right] F_l^{l_0}(R) = - \sum_{l'} \langle V \rangle_{l,l'}(R) F_{l'}^{l_0}(R) \quad (3)$$

where the collision energy, $E_{\text{coll}} = E - E_{v,j}$, where $E_{v,j}$

is the internal energy of the diatom. $\langle V \rangle_{l,l'}(R)$ desig-

nates the matrix elements in the SF basis of $V^0(R, r, \theta) - V_{\text{H}_2}(r)$, with $V_{\text{H}_2}(r)$ the asymptotic H_2 diatomic potential. By inwards integration of Eq. (3) we obtain the ‘‘regular’’ ($F_l^{(1)l_0}$) and ‘‘irregular’’ ($F_l^{(2)l_0}$) asymptotic radial wavefunctions, corresponding to an incoming (J, M, v_0, j_0, l_0) channel [10]. Let us note that, as can be seen in Eq. 3, $\langle V \rangle_{l_0, l_0}(R) + l_0(l_0 + 1)\hbar^2/2\mu R^2$ (diagonal part) has the meaning of the effective potential felt by the colliding partners at a distance R when approaching in the state $\varphi_{v_0 j_0 l_0}^{JM}$. Such meaning will be very useful below.

Regarding the calculation of the potential matrix $\langle V \rangle_{l, l'}(R)$, it is convenient to calculate the potential matrix associated to a basis labeled by the projection Ω_j of

\mathbf{J} on the Body–Fixed (BF) coordinate system whose z -axis is chosen along the Jacobi \mathbf{R} vector. This BF basis set is given by

$$\phi_{vj\Omega_j}^{JM} = \frac{\chi_{v,j}(r)}{r} \sqrt{\frac{2J+1}{4\pi}} D_{M\Omega_j}^{J*}(\alpha, \beta, \gamma) Y_{j\Omega_j}(\theta, 0), \quad (4)$$

where $\chi_{v,j}(r)$ is the radial rovibrational wave function, $Y_{j\Omega_j}(\theta, \phi)$ the spherical harmonics, and the $D_{M\Omega_j}^{J*}$ denotes a Wigner rotation matrix element where (α, β, γ) are the Euler angles corresponding to the transformation between SF and BF frames. It is easy to see that the matrix elements of the ground PES in this basis are thus given by

$$\langle V \rangle_{\Omega_j, \Omega'_j}(R) = \delta_{\Omega_j, \Omega'_j} 2\pi \int \chi_{v,j}^2(r) Y_{j\Omega_j}^2(\theta, 0) V^0(R, r, \theta) \sin \theta \, dr \, d\theta \quad (5)$$

Once the potential matrix elements are calculated in BF frame, we change to the S-F basis, which basically involves a combination with $3j$ symbols, thus obtaining

$$\langle V \rangle_{l, l'}(R) = (-1)^{l+l'} \sqrt{2l+1} \sqrt{2l'+1} \sum_{\Omega_j} \begin{pmatrix} j & l & J \\ \Omega_j & 0 & -\Omega_j \end{pmatrix} \begin{pmatrix} j & l' & J \\ \Omega_j & 0 & -\Omega_j \end{pmatrix} \langle V \rangle_{\Omega_j, \Omega_j}(R).$$

Finally, let us note that we have chosen an intermolecular separation of $\sim 10 \, a_0$ for the matching of the inner information with the asymptotic functions. The S-matrix has been calculated on a grid of 120 equally spaced energies in the collision energy range 0.09–10 meV (that is, for every ‘integer’ energy in the range from 1 to 120 K). Eighteen partial waves ($J = 0 - 17$) were required in order to converge the cross-sections in that energy range. Other convergence parameters used in the current work are the same which were used in the study of the title collision at thermal energies, and are given in ref. [15, 16].

III. RESULTS

Reaction cross-sections as a function of the collision energy (excitation function), $\sigma_R(E_{\text{coll}})$, for the $\text{S}(^1\text{D}) + \text{H}_2$ ($v=0, j=0$) collisions in the center-of-mass kinetic energy range 0.09–10 meV (1–120 K), have been calculated using the three methodologies described in the previous section. The calculations have been carried out on both the RKHS PES [14] and DMBE/CBS PES [30] versions of $\text{H}_2\text{S } ^1\text{A}'$ ground state PES. As stated above, the effects of singlet excited PESs and spin-orbit coupling are not considered here [10].

Fig. 1 depicts the accurate QM results for the excitation function on the two PESs. Although both curves have a similar shape and decay rapidly with the collision energy, the value of the cross section given by the RKHS

PES is about three times larger than that obtained on the DMBE/CBS. Remarkably, while the excitation function corresponding to RKHS displays a series of wide oscillations, as noted in our previous work on the system [2, 10], the results corresponding to the DMBE/CBS PES are in general smoother and only below 2 meV give rise to sharp peaks.

The comparison of the QM results with the excitation functions calculated using the other two dynamical approaches is shown in Fig. 2. For the DMBE/CBS PES (bottom panel), the QCT cross sections reproduce fairly well the smoothed out QM data for energies above 1 meV. As expected, the sharp structures observed below 5 meV, likely caused by long-lived resonances, are not accounted for by the classical calculations. In turn, the SQCT results are consistently higher than the QM data in the whole energy range. As in previous studies, the difference between QCT and SQCT results can be attributed to the failure of ergodicity for trajectories that overcome the centrifugal barrier but do not form a long-lived complex due to an inefficient transfer of momentum to the H_2 molecule. As can be seen, this difference is relatively small for the title reaction, although somewhat smaller on the DMBE/CBS PES. For the RKHS PES (upper panel) the SQCT cross sections are much closer to the exact QM results than those obtained with the QCT calculations. The fact that SQCT calculations underestimate the reactivity could suggest a significant presence of tunneling, as it will be discussed hereinafter. In spite of the differ-

ences between the results obtained with the QM, QCT and SQCT methods in each PES, all the calculations using any of these theoretical approaches predict a lower reactivity on the DMBE/CBS PES. Therefore it can be concluded that the major dynamical differences between the two PES cannot be attributed simply to quantum effects.

Further information on the remarkably different reactivity on the two PESs can be gained by inspection of the opacity functions; *i.e.*, the reaction probability as a function of the total (here also orbital) angular momentum, $P(J)$. Fig. 3 portrays the opacity functions obtained using the three methods for 5 meV, 10 meV and 30 meV collision energies. The differences in shape and magnitude between the opacity functions calculated on both PES are conspicuous. Not only the highest values of J accessible, J_{\max} , on the RKHS PES are considerably larger in the energy range here considered, but also the quantum reaction probabilities in the DMBE/CBS PES are smaller what justifies the big difference in the excitation functions. Similar effect occurs with the QCT and SQCT calculations except for the lower J values.

It is convenient to describe the results on the two PESs separately. Starting with the RKHS PES, the QM opacity function exhibits two regions depending on the J value. In the first one, the reaction probability oscillates around a high value, ~ 0.9 , suggesting a barrierless reaction, in which the energy is much bigger than the centrifugal barrier. In the second region, the opacity function decreases, manifesting a progressive hindrance for the reaction, until the reaction probability vanishes due to the inability to overcome the centrifugal barrier. The behavior of the SQCT opacity function is somewhat more complicated. The results corresponding to the higher collision energy, 30 meV, show also two regions but with different origin and located at different values of J than in the QM case. For low angular momenta, the opacity function has a value which is close to unity, but then, around $J=9$, gives rise to a sort of step at a constant value ~ 0.7 . Finally, by $J=20$, it briskly drops, to die at the same J_{\max} as the quantum opacity function. However, at $E_{\text{coll}}=5$ meV and 10 meV, the first region with $P(J) \approx 1$ is absent in the SQCT opacity functions which takes a constant value of 0.7 until it suddenly drops. Interestingly, the values of the SQCT probabilities in this region seem to be a lower limit for the oscillations of the QM ones. In contrast, in the range of J values of the second region where the QM probability decreases, the SQCT and QCT probabilities are bigger than the QM ones. As for the QCT results, the opacity functions exhibit essentially the same shape as the SQCT ones but with somewhat smaller values, analogously to what happened for the excitation functions. In particular, one can distinguish two regions at 30 meV but just one for lowest energies, as in the SQCT case.

The opacity functions on the DMBE/CBS PES are in strong contrast with those found on the RKHS PES. In general, they are smoother, decreasing gradually with in-

creasing J values, after an initial slight increase of the reaction probabilities. It is surprising that even for the lowest partial waves, the QM reaction probability at 5 meV is limited to ≈ 0.5 whereas for those calculated on the RKHS PES it was close to unity. In addition, for all the three energies, the values of J_{\max} are always lower than those corresponding to the calculations on the RKHS PES.

Summarizing, the main dynamical differences between the two PES in the considered energy range are: (a) The reactivity corresponding to the DMBE/CBS PES is much lower than that corresponding to the RKHS PES. In spite of the presumed barrierless character of the former, it seems that there is something that systematically hinders the reaction, even for low angular momenta where the centrifugal barrier is absent or small. (b) The shapes of the corresponding opacity functions are strikingly different on the two PESs. (c) The QM opacity functions and cross sections on the DMBE/CBS PES seem to oscillate around their QCT counterparts, and are in better agreement with each other than in the case of the results on the RKHS PES.

IV. DISCUSSION

As shown in a previous study [10], the reaction probability in the title reaction is essentially limited by the capture probability in the S+H₂ arrangement channel. In the energy range here considered, there is only one single open channel ($v=0, j=0, \Omega=0$) in the S+H₂ arrangement *vs.* 16 open rovibrational levels in the products with their corresponding Ω states. Consequently, according to the statistical model, which assumes the formation of an intermediate complex, the probability of complex breakdown into products is much larger than into reagents, and therefore the reaction probability is essentially equal to the capture probability from the initial state. We shall prove that indeed the reactivity is dominated by the dynamical features of the entrance channel and provide a neat explanation of the differences observed in the calculations on the two PES.

Let us start discussing the QM results on the RKHS PES and their comparison with the SQCT data. As it has been shown, the QM opacity function has a marked oscillating behavior for all the energies here considered. These oscillations were also found when examining the reaction probabilities as a function of the collision energy (not shown here) for a fixed J [15]. Even for $J=0$, where there is no centrifugal barrier, reaction probabilities in this system do not reach the unity in the considered energy range except for very particular energies, but quickly oscillate around an average of ≈ 0.9 . This behavior is a manifestation of an indirect mechanism mediated by resonances which is characteristic of the presence of the deep well supporting the SH₂ collision complex. Except for the fact that the oscillations become somewhat more shallow and that, on average, the reaction proba-

bility is closer to one, the effect of raising E_{coll} does not bring any substantial change with respect to the lower energies here examined.

In contrast, as commented on above, the SQCT results at the two lowest E_{coll} here presented give rise to a very flat reaction probability, essentially constant with J , up to a value wherein $P(J)$ drops suddenly and becomes zero. Interestingly, the reaction probability in this flat region is ≈ 0.7 . The fact that the SQCT approach underestimates the reactivity in this range of J as compared to the QM method indicates that some of the incoming flux is classically reflected before the capture can take place, while in the QM case those collisions lead, however, to complex formation. This behavior can only be explained by the contribution of tunneling.

In order to explain such behavior it is pertinent to examine the topography of the entrance channel of the two PESs. We have already stated that the big differences in reactivity when comparing both PESs are a consequence of a significant difference in the J_{max} value of the opacity functions in both QM and classical results, together with lower reaction probabilities in the case of the DMBE/CBS PES in the whole range of J . However, the difference in the reactivity cannot be associated with a dynamical behavior inside the potential well as long as the SQCT and QCT calculations render similar opacity functions and, in particular, identical values of J_{max} . Since trajectories in the SQCT calculations do not explore the well, the discrepancy between the results on the two PESs must be primarily due to features located in the entrance valley before the deep insertion well.

Fig. 4 displays contour plots of the entrance channel of the PESs for specific H–H internuclear distances, r . The selected r values correspond to the H_2 equilibrium distance, r_{eq} , and to the inner, r_- , and outer, r_+ , classical turning points for the $(v=0, j=0)$ and $(v=1, j=0)$ rovibrational states. Cuts are drawn as a function of R_x and R_y , where R_x and R_y are the projections of the Jacobi atom-diatom distance, R , onto the three atom plane, with the x -axis along the H_2 molecular axis. Specifically, the left panels correspond to the RKHS PES and the right panels to the DMBE/CBS PES. Common to all these plots is the presence of the insertion well (negative green contours) at perpendicular geometries centered at $R \approx 1.4$ Å. Red contours indicate the repulsive, inner part of the potential. In addition, the presence of a relatively small barrier at the collinear configuration can be observed in most of the plots, and it seems especially significant at the H_2 equilibrium distance. Although there are general resemblances between the two PESs at the various H_2 distances, there are features which are clearly different. In the case of the RKHS PES, for $r < r_{\text{eq}}$, the collinear barrier is clearly broader than that for $r = r_{\text{eq}}$, whereas for $r > r_{\text{eq}}$, the width decreases until it finally disappears. In the DMBE/CBS PES, the collinear barrier is much more confined and persists for all values of $r > r_{\text{eq}}$, and, in contrast to the RKHS PES, it grows with the H–H bond stretching. Most interestingly though, is the fact

that for configurations implying a compressed H–H bond, the barrier grows considerably and covers a broad range of R values and orientations of the H_2 molecule. Finally, it is worth mentioning the existence of a shallow van der Waals well (43 meV depth) at $R \approx 3.5$ Å (light green external regions) in the RKHS PES which is not evident in the DMBE/CBS PES. As will be seen, both, the barrier and the van der Waals well ref. [19], play important roles in the dynamics at low collision energies.

Returning to the discussion of the dynamics on the RHKS PES, tunneling through the aforementioned barrier is likely to occur. For high angular momenta, with significant centrifugal barriers, tunneling through the combined dynamical and centrifugal barrier gives rise to shape resonances which survive the sum over partial waves and can be observed at some specific energies, causing marked oscillations in the excitation function [2, 10]. A nice example of these shape resonances is depicted in Fig. 5 at $E_{\text{coll}}=6.26$ meV, at which a marked oscillation in the RKHS excitation function takes place (see Fig. 1). The raise of the $P(J)$ for $J=15$, which is classically closed, leads to a substantial increase in the cross section. Therefore, although the values of J_{max} for QM results has been shown to usually coincide with those found in the SQCT or QCT calculations (see Fig. 3), this is not the case at some specific energies, as that shown in Fig 5. This is a clear case of a genuine quantum effect that none of the classical approaches can account for.

An interesting finding is the step for $J=9$ in the SQCT $P(J)$ at $E_{\text{coll}}=30$ meV, which marks the transition from $P(J)=0.7$ to $P(J)=1.0$ (see Fig. 3). This step is absent at lower collision energies wherein the maximum value of $P(J)$ is always 0.7. The observation of the plots of Fig. 4 provides an explanation for this behavior. As can be seen, at the low collision energies considered, the approach to the deep attractive well is only impeded by the small “ear-shape” barrier near collinearity at $R \approx 2.5$ Å. Its net effect is to partially screen the well making the reaction probability be less than one. That is, at sufficiently low E_{coll} the cone of acceptance is limited to those configurations for which the dynamical barrier is null, what approximately amounts 70% of the collisions. This explains why $P(J)$ is flat for a given range of J , until a value for which the centrifugal barrier is higher than the collision energy, and then it drops to zero. The appearance of a region where $P(J)=1$ with increasing energy (at $E_{\text{coll}} \geq 30$ meV) clearly indicates that the radial energy is sufficient to overcome the dynamical barrier and the cone of acceptance practically covers 100%. Nevertheless, with increasing J , and thus with a higher centrifugal barrier, the situation reverts to that observed at lower energies; namely, there are directions of approach for which the reaction cannot take place thus reducing the reaction probability.

The above discussion serves to explain the classical behavior. However, the QM reaction probabilities cannot be accounted for by the same rationale. Apart from the oscillations and the energetically localized resonances as

that shown in Fig. 5, the $P(J)$ have consistently higher values (that can reach the unit for some J values) than those calculated by the SQCT method, and, in fact, the SQCT provides a lower limit for the QM reaction probabilities. In addition, somehow surprisingly, the fall of the QM $P(J)$ is more gradual than in the classical case and leads to the apparent paradox that for high J the SQCT (and QCT) $P(J)$'s are higher than the QM ones in a sort of paradoxical “anti-tunneling” behavior.

The situation becomes clear in the light of the 1D quantum effective potentials, $\langle V(R) \rangle_{l,l} + l(l+1)\hbar^2/2\mu R^2$, calculated as indicated in Section IIC. It must be stressed that they are constructed by averaging the $V^0(R, r, \theta)$ over r and θ using the rovibrational state as a probability distribution and adding the centrifugal term. Figure 6 portrays the effective potentials for the RKHS PES (upper panel) and the DMBE/CBS PES (lower panel). Note the presence in general of two barriers, one external, relatively blunt, and a very sharp inner one. In the case of the RKHS PES, the origin of the external barrier is clear as long as it is absent in the $J=0$ effective potential, and therefore can be attributed to the centrifugal barrier. The inner, sharp barrier has its origin in the collinear barrier mentioned above. As a matter of fact, this feature would not be present if only the insertion approach had been considered. The interplay of these two barriers explains the two regimes observed in the QM opacity functions. Taking the 5 meV case as an example, as long as the effective potential stays below the collision energy (until $J=12$), the system can access the well without hindrance and reacts. The QM $P(J)$ reaches high probabilities (on average, close to one) in what we have called the QM first region. In this regime, the external barrier is always larger than the internal one, and we can think of it as the ‘bottleneck’ which limits the flux entering into the well. However, for $J = 13$, it is the internal barrier the one which starts blocking the access to the well at the considered energy, in coincidence with the decay of the opacity function. In this regime, the reaction occurs via tunneling through the inner (thin) barrier. Finally, for $J = 14$, both the external and the internal centrifugal barriers are higher than the kinetic energy, and the opacity function essentially vanishes. In summary, the two regimes of QM opacity functions are closely related to the maxima in the effective potential. Let us also remark that it is precisely this double maximum structure comprising a local minimum, (see Fig. 6) the one which supports the above mentioned shape resonances for particular partial waves. These resonances are the origin of some of the oscillating structures in the QM excitation functions, as commented on above and discussed in a previous work [10].

The presence of the second, inner, barrier in the effective potentials of the RKHS PES sheds light on the somewhat surprising “anti-tunneling” behavior. In the classical picture, a trajectory *feels* only the local value of the potential at the points the trajectory is going through. In the quantum picture, the system is sensitive

to the average (thus ‘non local’) value of the potential. As the potential has to be averaged over the whole angular range (and over internuclear distances), the distinction between the directions of approach with and without barrier loses its meaning. Effectively, except for tunneling, this situation would be equivalent to that resulting from a QCT calculation with an isotropic potential than would be smaller than the local value of the barrier. In that case, the SQCT $P(J)$ will be zero just at the J value in which the QM ones start decreasing. While classically the hindrance in reactivity is understood as a fractional closure of reactive configurations, the process can be described in quantum mechanical terms as a decreasing tunneling through an increasing barrier.

As shown hereinbefore, the opacity functions calculated on the DMBE/CBS (see Fig. 3) are strikingly different, and it seems that the previous arguments could not be valid to explain those results. In fact, the SQCT reaction probabilities constitute an upper limit for the QM results at the three energies examined. Let us consider now the effective potential in the case of the DMBE/CBS PES. Surprisingly, the presence of a very high and sharp internal barrier could limit the access to the well even for $J = 0$. This dynamical internal barrier, in an apparently *barrierless* reaction, must be the reason for the much lower QM reaction probabilities. Its origin will be justified below. Comparing the QM $P(J)$ at 5 meV with the plot of the effective potential, it becomes clear that it is the height of the external barrier what determines the J_{\max} accessible for the reaction to take place. For a given J , this external barrier is always lower for the RKHS PES than for the DMBE/CBS PES, what justifies the larger J_{\max} in the former. In addition, the inner barrier is much higher in the case of the DMBE/CBS PES even for $J=0$, and becomes broader with increasing J to the point of collapsing with the outer barrier into a single crest at $J \approx 15$ (not shown). In addition, for $J < 15$ the well between the maxima is more shallow than in the RKHS PES. The features of the PES responsible of the inner barrier have to be the origin of the also much smaller reactivity in the classical treatments.

At this point, we need to return to Fig. 4 to relate the topography of the PES to the two remarked features of the effective potentials: (i) the more pronounced minimum between maxima in the case of the RKHS PES, responsible for the higher J_{\max} , and (ii) the high inner barrier present in the DMBE/CBS PES, responsible for the much smaller values of reaction probabilities even for $J = 0$.

With regard to the feature (i), it can be shown that the minimum in the effective potential of the RKHS PES relies on the aforementioned van der Waals, mostly absent in the DMBE/CBS PES. Far from being an artifact of the fit, this well seems to be real, appearing also in some *ab initio* calculations performed to verify its existence [10], although with smaller depth. It is also the origin of many of the structures in the cross-sections of the RKHS PES and of the decrease of height of the centrifugal barriers.

As for the feature (ii), the origin of the high inner barrier in the effective potential of the DMBE/CBS PES can be traced back to the nearly isotropic barrier that appears as the H–H bond starts to be compressed. This barrier covers a broad range of R between 1.5 and 4.5 Å, as shown in Fig. 4, and its height is strongly dependent on the value of r . For T-shape configuration it may become very significant; as high as 200 meV at the inner turning point for $v=0$ and surpassing 1 eV for the inner turning point of $v=1$. This remarkable feature is basically absent in the RKHS PES.

The much lower reactivity of the DMBE/CBS can thus be attributed to this barrier to the extent that actually the global PES is not truly barrierless. As a result of this, the reaction probability calculated on this PES decreases gradually with the impact parameter, as shown in Fig. 3, and the shape of the opacity functions at sufficiently low collision energies calculated by any of the three methodologies deviates considerably from what can be expected for a typical barrierless reaction, as typified by the corresponding results on the RKHS PES. It must be stressed that the mentioned barrier only appears for compressed H–H bond configurations and its maximum height turns up at $R \approx 2.2$ Å.

It can be expected that the effect of this barrier will show up blatantly for the reaction with vibrationally excited molecules for which the H_2 internuclear distance can reach shorter values. In particular, the corresponding QCT and SQCT excitation functions for the reaction with $H_2(v=1, j=0)$ are shown in Fig. 7 in the 25–300 meV collision energy range. The $\sigma_R(E_{\text{coll}})$ calculated on the RKHS PES follows the expected behavior: a shape, monotonically decreasing with E_{coll} , and absolute values similar to those obtained in the reaction with $H_2(v=0, j=0)$. In strong contrast but at this point not surprisingly, the QCT and SQCT excitation functions calculated on the DMBE/CBS exhibit a threshold at $E_{\text{coll}} \approx 25$ mV. The shape of the excitation functions is akin to that of a reaction with barrier. Only at sufficiently high E_{coll} the values of $\sigma_R(E_{\text{coll}})$ become comparable to the results found for the reaction with $H_2(v=0, j=0)$.

The opacity functions corresponding to 32 meV and 82 meV calculated on both PESs are shown in Fig. 8. The results obtained on the RKHS (upper panels) are similar to those found at $E_{\text{coll}}=30$ meV for $v=0, j=0$, displaying two distinct regimes; a first one with higher reaction probabilities ≈ 0.9 and, a second one that appears as a notch before the sudden drop to zero. It is worth noticing that the maximum value of the SQCT $P(J)$ is somewhat smaller than that obtained in the reaction with H_2 in $v=0$ due to a larger probability of complex breakdown into reactants as the total energy increases. The results on the DMBE/CBS PES clearly indicate lower reaction probabilities than in the case of the $v=0$. Interestingly, vibrational excitation does not promote but hampers the reactivity.

Let us finally note that as stated in ref. 30, the

grid of *ab initio* points used for the construction the DMBE/CBS PES sampled the S- H_2 entrance channel for H–H internuclear distances in the $1.4a_0 \leq r \leq 3.4a_0$ range. In view of this sampling, and being the equilibrium distance of H_2 precisely $1.4 a_0$ we may conclude that the observed repulsive barrier is likely an artifact of the fit of the PES, perhaps reflecting the lack of electronic structure calculations for short H–H internuclear distances. This work is then illustrative of the conflicting objectives that are present when modeling a PES. If the electronic structure calculations can be done accurately and expediently, numerical or semi-numerical interpolation schemes can be utilized to reproduce the subtle details that govern nuclear dynamics on single-sheeted PESs, as is the case with the RKHS H_2S PES. This is so, even if extrapolation to the asymptotes can somewhat endanger the analysis. However, when accurate calculations are just hardly affordable, then a least-squares fit based whenever possible on a physically motivated form like DMBE that can be calibrated from a relatively small number of *ab initio* points may be ideal. Such a dilemma poses itself a compromise that has been well illustrated in the present case study. In fact, the major goal of Ref. 30 has been to test, to our knowledge for the first time, a general cost-effective methodology [31, 41] to generate accurate global PESs using traditional correlated *ab initio* methods and basis sets with low cardinal numbers. The focus has then been on the quality of the calculated energies, by limiting their number to a minimum level, while relying mostly on the predicting capability of the DMBE formalism to generate the global PES. Clearly, if subtle topographical features are at stake, the method should be used with caution. This can be done either via a gradually increase of the size of the grid of *ab initio* points until definite trends are observed or by joint use of dynamics calculations, which may hopefully suggest additional *ab initio* calculations by alerting for critical predictions and hence for the sparseness of the grid at specific regions of configuration space [42, 43]. It should be recalled that, interestingly, fits based on similar forms but using slightly different grid sizes may lead to different results, mostly when possessing excessive flexibility. In fact, even if such differences can be minor and hardly visible, they can be made to play a key role if specific energy regimes are devised, such as the case with the low collision energies here considered. Indeed, this has been exemplified for H_2S , with the fitting artifacts reported here (and elsewhere [34, 44]) for the DMBE/CBS PES. These features essentially disappear when considering the DMBE/SEC PES [32], in spite of the fact that both basically employ the same grid of *ab initio* energies as calibration data. Thus, the release of a global PES prior to use with a sufficiently demanding test set of dynamics calculations runs the risk of failure whenever a property outside the test set is considered. This has been the case with the DMBE/CBS PES for which a recalibration is desirable. Similarly, even if they are seemingly small, a careful evaluation of non-adiabatic ef-

fects for the title system is imperative thus requiring the modeling of a multi-sheeted PES.

V. CONCLUSIONS

Detailed quantum mechanical (QM), quasi-classical (QCT) and statistical (SQCT) calculations have been performed for the $S(^1D)+H_2(v=0, j=0)$ insertion reaction on two different PESs in the 0.09–10 meV collision energy range. Although the differences between the results obtained with the three methodologies are appreciable, the QCT and SQCT are in a general good agreement with the accurate single PES QM calculations. In particular, the good agreement between SQCT and the accurate QM calculations lends credence to the tenet that the reaction is limited by the capture probability in the entrance channel, and that the formation of a the collision complex takes place once the centrifugal barrier is surmounted. As such, for this type of reactions, the study of collisions at very low translational energies may be a sensitive probe of the detailed topography of the entrance channel and the long-range part of the PES.

Even though it can be expected that the amount of reactive flux should be mostly determined by the purely centrifugal barrier, rather subtle topographical features localized in specific regions of the PES may influence on the reactivity at low energies. Indeed, the three sets of calculations show unequivocally that the reactivity on the RKHS PES is much larger than that obtained on the more recent DMBE/CBS PES. In fact, the opacity functions determined on the two PESs are remarkably different in shape and in absolute value, and reveal that the lower reactivity on the DMBE/CBS PES is due to lower values of the reaction probability in practically the whole range of orbital angular momenta (or impact parameters), as well as to considerably smaller values of maximum impact parameter leading to reaction.

The detailed inspection of the opacity functions and the comparison of the SQCT and QM results provides important clues on the detailed dynamics of the reaction on each PES. As a matter of fact, the shape and absolute values of the reaction probabilities have been explained in terms of the topography of the PES and, in particular, of the corresponding effective potential in the entrance channel, which are averaged over the internuclear distances and orientations of the H–H molecule. In the case of the RKHS, it has been shown that the small collinear barrier, whose influence at higher energies is very minor, plays a significant role on the features found in the opacity functions at small collision energies. In the case of the the DMBE/CBS PES, the huge differences found in the reaction probabilities with respect to those on the RKHS PES can be attributed to the presence of a barrier that becomes very significant when the H–H bond is compressed, a region of the PES wherein *ab initio* data were largely missing.

To confirm the hampering role for the reaction to oc-

cur associated with this barrier at small H–H internuclear distances, QCT and SQCT calculations of cross sections and opacity functions were also carried out for vibrationally excited H_2 in $v=1$. Whilst on the RKHS the excitation function is analogous to that found for $v=0$, in the case of the DMBE/CBS not only the cross-section for $v=1$ is lower than that for $v=0$ but also gives rise to a reaction threshold, a clearly unexpected feature for a barrierless reaction.

This work shows that the study of presumably barrierless reactions at low collision energies ($< 100K$) can reveal features in the global PES that would have been unnoticed at higher energies. These features can and indeed do affect the dynamics of the reaction whose accurate description is mandatory to undertake studies at the cold and ultracold regimes as it has long been anticipated [45] but not demonstrated as clearly as here done via rigorous classical and quantum dynamics calculations on accurate *ab initio* based PESs. Indeed, the present study can be illuminating about the difficulties encountered in modeling an all-purpose global potential energy surface.

Acknowledgments

The support of the Spanish Ministry of Science and Innovation (grants CTQ2008-02578/BQU and Consolider Ingenio 2010 CSD2009-00038) are gratefully acknowledged. PGJ acknowledges the FPU fellowship AP2006-03740. AJCV thanks the support of Fundao para a Ciencia e a Tecnologia, Portugal.

-
- [1] A. Canosa, F. Goulay, I. R. Sims, and B. R. Rowe, *Low Temperatures and Cold Molecules* (World Scientific, Singapore, 2008).
- [2] C. Berteloite, M. Lara, A. Bergeat, S. D. Le Picard, F. Dayou, K. M. Hickson, A. Canosa, C. Naulin, J.-M. Launay, I. R. Sims, et al., *Phys. Rev. Lett.* **105**, 203201 (2010).
- [3] M. Lara, F. Dayou, J.-M. Launay, A. Bergeat, K. M. Hickson, C. Naulin, and M. Costes, *Phys. Chem. Chem. Phys.* **13**, 8127 (2011).
- [4] I. R. Sims and M. Costes (2010), personal communication.
- [5] A. J. C. Varandas, *Adv. Chem. Phys.* **74**, 255 (1988).
- [6] A. J. C. Varandas, *Conical Intersections: Electronic Structure, Spectroscopy and Dynamics* (World Scientific Publishing, 2004), chap. 5, p. 91, Advanced Series in Physical Chemistry.
- [7] P. F. Weck and N. Balakrishnan, *Int. Rev. Phys. Chem.* **25**, 283 (2006).
- [8] S. Ospelkaus, K.-K. Ni, D. Wang, M. H. G. de Miranda, B. Neyenhuis, G. Quémener, P. S. Julienne, J. L. Bohn, D. S. Jin, and J. Ye, *Science* **327**, 853 (2010).
- [9] P. Julienne, *Faraday Discuss.* **142**, 361 (2009).
- [10] M. Lara, F. Dayou, and J.-M. Launay, *Phys. Chem. Chem. Phys.* **13**, 8359 (2011).
- [11] F. J. Aoiz, L. Bañares, and V. J. Herrero, *J. Phys. Chem. A* **110**, 12546 (2006).
- [12] A. S. Zyubin, A. M. Mebel, S. D. Chao, and R. T. Skodje, *J. Chem. Phys.* **114**, 320 (2001).
- [13] S. D. Chao and R. T. Skodje, *J. Phys. Chem. A* **105**, 2474 (2001).
- [14] T.-S. Ho, T. Hollebeek, H. Rabitz, S. D. Chao, R. T. Skodje, A. S. Zyubin, and A. M. Mebel, *J. Chem. Phys.* **116**, 4124 (2002).
- [15] L. Bañares, F. J. Aoiz, P. Honvault, and J.-M. Launay, *J. Phys. Chem. A* **108**, 1616 (2004).
- [16] L. Bañares, J. F. Castillo, P. Honvault, and J.-M. Launay, *Phys. Chem. Chem. Phys.* **7**, 627 (2005).
- [17] P. Honvault and J.-M. Launay, *Chem. Phys. Lett.* **370**, 371 (2003).
- [18] E. J. Rackham, T. González-Lezana, and D. E. Manolopoulos, *J. Chem. Phys.* **119**, 12895 (2003).
- [19] F. J. Aoiz, T. González-Lezana, and V. S. Rábanos, *J. Chem. Phys.* **129**, 094305 (2008).
- [20] T. González-Lezana, *Int. Rev. Phys. Chem.* **26**, 29 (2007).
- [21] S. Y. Lin and H. Guo, *J. Chem. Phys.* **122**, 074304 (2005).
- [22] J. A. Klos, P. J. Dagdigian, and M. H. Alexander, *J. Chem. Phys.* **127**, 154321 (2007).
- [23] B. Maiti, G. C. Schatz, and G. Lendvay, *J. Phys. Chem. A* **108**, 8772 (2004).
- [24] S.-H. Lee and K. Liu, *J. Phys. Chem.* **102**, 8637 (1998).
- [25] S.-H. Lee and K. Liu, *Chem. Phys. Lett.* **290**, 323 (1998).
- [26] S.-H. Lee and K. Liu, in *Advances in Molecular Beam Research and Applications* (Springer-Verlag, Berlin, 2000).
- [27] T.-S. Chu, K.-L. Han, and G. C. Schatz, *J. Phys. Chem. A* **111**, 8286 (2007).
- [28] H. Yang, K.-L. Han, G. C. Schatz, S.-H. Lee, K. Liu, S. C. Smith, and M. Hankel, *Phys. Chem. Chem. Phys.* **11**, 11587 (2009).
- [29] E. J. Rackham, F. Huarte-Larranaga, and D. E. Manolopoulos, *Chem. Phys. Lett.* **343**, 356 (2001).
- [30] Y. Z. Song and A. J. C. Varandas, *J. Chem. Phys.* **130**, 134317 (2009).
- [31] A. J. C. Varandas, *J. Chem. Phys.* **126**, 244105 (2007).
- [32] Y. Z. Song, P. J. S. B. Caridade, and A. J. C. Varandas, *J. Phys. Chem. A* **113**, 9213 (2009).
- [33] A. J. C. Varandas, *J. Chem. Phys.* **90**, 4379 (1989).
- [34] M. Hankel, S. C. Smith, and A. J. C. Varandas, *Phys. Chem. Chem. Phys.* **00**, (in press) (2011).
- [35] F. J. Aoiz, V. J. Herrero, and V. Sáez Rábanos, *J. Chem. Phys.* **97**, 7423 (1992).
- [36] F. J. Aoiz, L. Bañares, and V. J. Herrero, **94**, 2483 (1998).
- [37] F. J. Aoiz, V. Sáez Rábanos, T. González-Lezana, and D. E. Manolopoulos, *J. Chem. Phys.* **126**, 161101 (2007).
- [38] F. J. Aoiz, T. González-Lezana, and V. Sáez-Rábanos, *J. Chem. Phys.* **127**, 174109 (2007).
- [39] J. M. Launay and M. L. Dourneuf, *Chem. Phys. Lett* **169**, 473 (1990).
- [40] P. Honvault and J.-M. L. Dynamics, in *Theory of Chemical Reaction Dynamics* (NATO Science Series vol. 145, Kluwer, 2004).
- [41] A. J. C. Varandas, *Chem. Phys. Lett.* **443**, 398 (2007).
- [42] M. J. T. Jordan, K. C. Thompson, and M. A. Collins, *J. Chem. Phys.* **102**, 5647 (1995).
- [43] K. C. Thompson, M. J. T. Jordan, and M. A. Collins, *J. Chem. Phys.* **108**, 8302 (1998).
- [44] M. Hankel, S. C. Smith, and A. J. C. Varandas, *Physica Scripta (CAMOP)* **00**, (in press) (2011).
- [45] A. J. C. Varandas, *J. Mol. Struct. Theochem* **166**, 59 (1988).

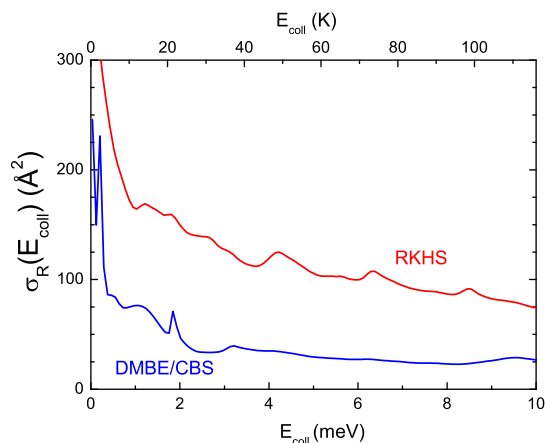


FIG. 1: (color online) Comparison of the QM total cross section as a function of the collision energy (excitation function) for the $S(^1D) + H_2(v=0, j=0)$ reaction calculated on the RKHS PES (red line) and DMBE/CBS PES (blue line). The upper energy scale is in K ($1 \text{ meV} \sim 11.6 \text{ K}$)

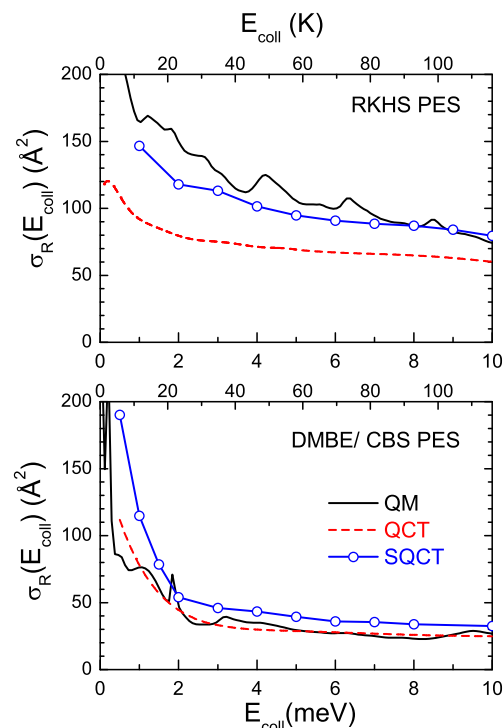


FIG. 2: (color online) Comparison of the excitation functions calculated using the QM, QCT, and SQCT methods. Top: Results on the RKHS PES. Bottom: Results on the DMBE/CBS PES. Solid (black) line, QM data; dashed (red) line, QCT results; solid (blue) line with open circles, SQCT results. The upper energy scale is in K.

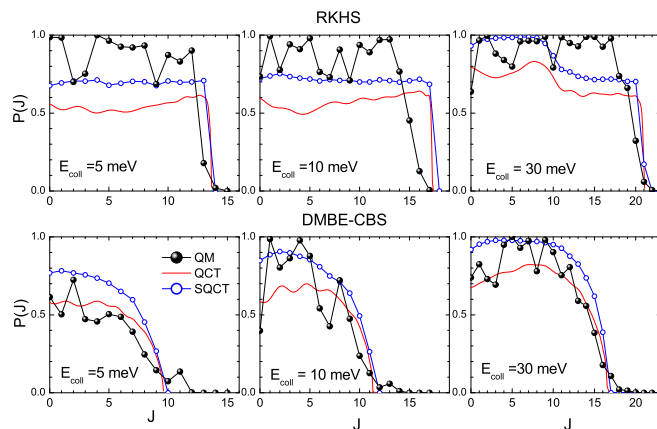


FIG. 3: (color online) Comparison of opacity functions for the $S(^1D) + H_2(v=0, j=0) \rightarrow SH + H$ reaction calculated using accurate QM (black solid lines with filled circles), QCT (red line) and SQCT (blue line with open circles) approaches at three specified kinetic energies. Upper panels correspond to the results obtained using the RKHS PES. Lower ones correspond to the results obtained using the DMBE/CBS PES.

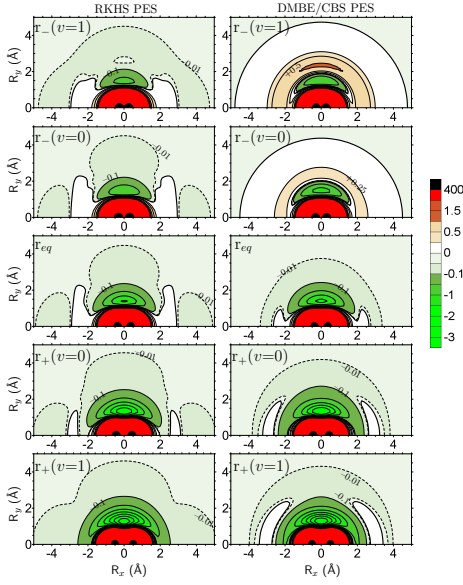


FIG. 4: (color online) Contour plots of the RKHS PES (left column) and DMBE/CBS PES (right column) at the H–H internuclear distances corresponding to the inner turning points, $r_-(v=1)$ (top row), $r_-(v=0)$ (second row), equilibrium distance, r_{eq} , (third row), outer turning points, $r_+(v=0)$ (fourth row), and $r_+(v=1)$ (bottom row). R_x is the components of the \mathbf{R} Jacobi vector (R_{S-H_2}) along the internuclear x axis. For each plot the zero of the energy scale corresponds to the asymptotic reactant’s valley at the indicated H–H distance (0 for r_{eq} , 0.27 eV for $r_{\pm}(v=0)$ and 0.78 eV for $r_{\pm}(v=1)$). Green contours indicate energies below the minimum of the S–H₂ valley. Red contours represent highly repulsive parts of the PES. The thick black contour represents the zero energy value that limits the “ear-like” barrier at collinear configurations. Notice the nearly isotropic barrier that appears in the DMBE/CBS PES for the compressed H–H bond.

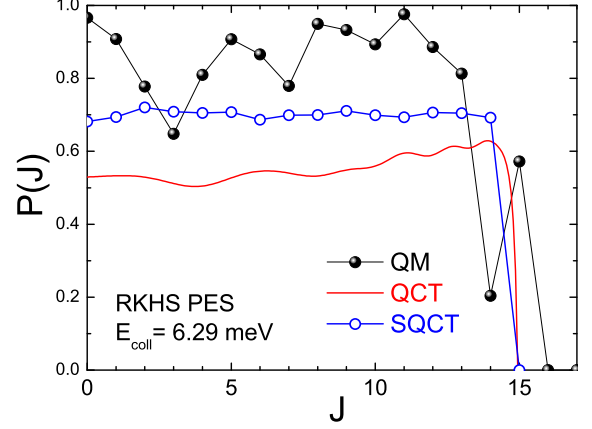


FIG. 5: (color online) Comparison of QM, QCT, and SQCT opacity functions calculated on the RKHS PES at $E_{\text{coll}}=6.26$ meV ($=73$ K). At this energy a shape resonance can be observed for $J=15$. See Fig. 1 and ref. 10. Lines and symbols as in Fig. 3.

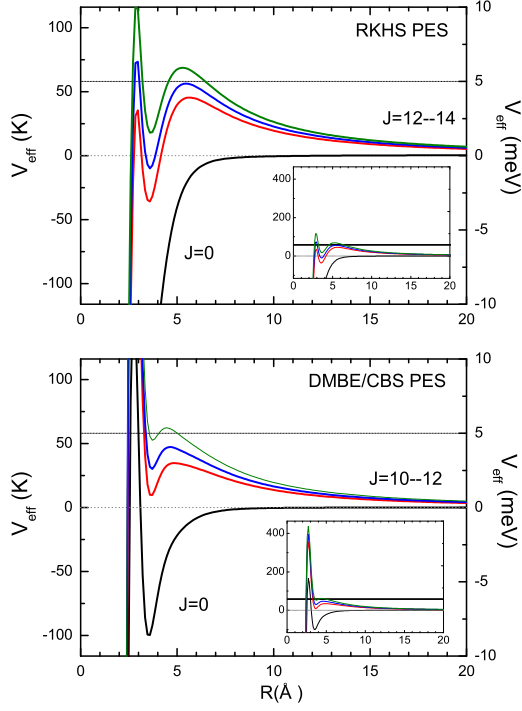


FIG. 6: (color online) Effective potentials, $\langle V \rangle_{l,l}(R) + l(l+1)\hbar^2/2\mu R^2$, averaged over the internuclear distance and orientation of $\text{H}_2(v=0, j=0)$ molecule. Upper panel: results on the RKHS PES. Lower panel: results on the DMBE/CBS PES. Note the presence of a sharp inner barrier and another outer barrier at larger distances. The minimum between these barriers in RKHS PES may support shape resonances. In the case of surface DMBE/CBS, the inner barrier is very high and it is present even for $J=0$ (see inset).

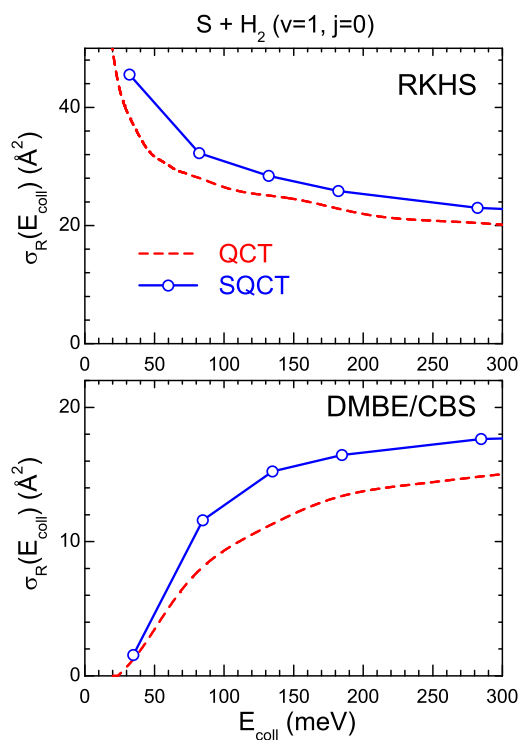


FIG. 7: (color online) Comparison of excitation functions for the $S(^1D) + H_2(v=1, j=0) \rightarrow SH + H$ reaction calculated with the QCT (red, dashed line) and SQCT (blue open circles) approaches on the RKHS PES (top) and DMBE/CBS PES (bottom). Note the different scales in each plot.

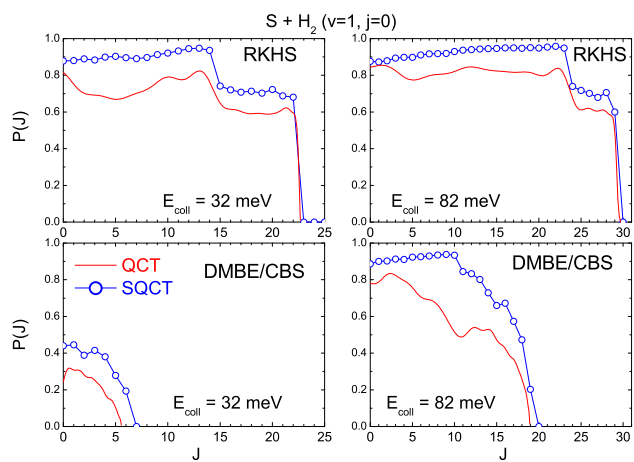


FIG. 8: (color online) Opacity functions for the reaction with $\text{H}_2(v=1, j=0)$ at 32 meV (left panels) and 82 meV (right panels) collision energy calculated with the QCT and SQCT approaches on the RKHS PES (top panels) and DMBE/CBS PES (bottom panel). These collision energies correspond to the first two points of the excitation functions of Fig. 7 calculated with the SQCT method. Lines and symbols as in Fig. 3.